Chemical Detection by Analyte-Induced Change in Electrophoretic Deposition of Gold Nanoparticles

Journal of The Electrochemical Society, 2022 **169** 016504
1945-7111/2022/169(1)/016504/6/$40.00 © 2022 The Electrochemical Society ("ECS"). Published on behalf of ECS by IOP Publishing Limited

Chemical Detection by Analyte-Induced Change in Electrophoretic Deposition of Gold Nanoparticles

Badri P Mainali and Francis P Zamborini[z]

Department of Chemistry, University of Louisville, Louisville Kentucky 40292, United States of America

The electrophoretic deposition (EPD) of citrate-stabilized Au nanoparticles (cit-Au NPs) occurs on indium tin oxide (ITO)-coated glass electrodes upon electrochemical oxidation of hydroquinone (HQ) due to the release of hydronium ions. Anodic stripping voltammetry (ASV) for Au oxidation allows the determination of the amount of Au NP deposition under a specific EPD potential and time. The binding of Cr^{3+} to the cit-Au NPs inhibits the EPD by inducing aggregation and/or reducing the negative charge, which could lower the effective NP concentration of the cit-Au NPs and/or lower the electrophoretic mobility. This lowers the Au oxidation charge in the ASV, which acts as an indirect signal for Cr^{3+}. The binding of melamine to cit-Au NPs similarly leads to aggregation and/or lowers the negative charge, also resulting in reduction of the ASV Au oxidation peak. The decrease in Au oxidation charge measured by ASV increases linearly with increasing Cr^{3+} and melamine concentration. The limit of detection (LOD) for Cr^{3+} is 21.1 ppb and 16.0 ppb for 15.1 and 4.1 nm diameter cit-Au NPs, respectively. Improving the sensing conditions allows for as low as 1 ppb detection of Cr^{3+}. The LOD for melamine is 45.7 ppb for 4.1 nm Au NPs.
 [DOI: 10.1149/1945-7111/ac418c]

Manuscript submitted October 17, 2021; revised manuscript received December 3, 2021. Published January 6, 2022. *This paper is part of the JES Focus Issue on Modern Electroanalytical Research in the Society for Electroanalytical Chemistry (SEAC).*

Supplementary material for this article is available online

Chromium is widely used in electroplating, dyestuff, leather tanning, metallurgy[1,2] and catalysis. As a consequence, chromium is released to the environment, causing a serious threat to human health.[3,4] Cr(VI) is biotoxic, while Cr(III) is important in the activation of glucose and metabolism of proteins and lipids.[1,5] However, excess Cr(III) intake induces oxidation of cellular components, such as DNA, proteins and lipids, leading to an increased risk of cardiovascular diseases, diabetes, and cancer.[6,7] Studies also show that Cr(III) is highly bioaccumulative and bioconvertible in nature, which causes considerable cell and tissue damage.[8,9] Interconversion of the two ionic forms of Cr is common via simple oxidation-reduction processes.[2,10,11] For these reasons, the detection of Cr(III) is necessary for environmental monitoring, including water and food safety.

Melamine ($C_3H_6N_6$) has applications as water-reducing agents, fire retardants, plastics, laminates, paints, and fertilizer mixtures.[12] Some food processing companies deliberately use melamine as a food additive to enhance the protein content.[13,14] However, since melamine is biotoxic in nature, it can cause many food borne diseases associated with the urinary tract and renal failure.[15,16] For example, melamine is able to form an insoluble complex with cyanuric acid, which is associated with kidney malfunction.[13] The recommended melamine concentration level in food is 2.5 mg kg^{-1} (2.5 ppm), with the daily melamine intake not exceeding 0.2 ppm of human body weight.[17] Therefore, there is an increasing demand for feasible, reliable, and sensitive methods to detect the melamine concentration in food and the environment.

The determination of Cr and melamine has been achieved previously by spectroscopic,[18–22] chromatographic,[23] colorimetric,[24–26] and electrochemical[27–29] methods. Spectroscopic and mass spectrometry methods, such as inductively-coupled plasma mass spectrometry (ICP-MS) and atomic absorption spectroscopy (AAS), involve sophisticated instrumentation, complex sample preparation, time consumption, and high cost.[30] Several researchers have employed Au NPs for the selective and sensitive detection of Cr and melamine by colorimetric methods.[31–33] This is possible due to the plasmonic properties of Au NPs, which provides them with a high extinction coefficient.[34] Detection is based on variation in absorbance and shift in the localized surface plasmon resonance (LSPR) band due to analyte-induced Au NP-Au NP interactions or aggregation. For example, Dong *et al.* detected Cr(III) and Cr(VI) by using gallic acid-capped Au NPs in the presence of citrate, thiosulphate, and ethylene diamine tetraacetic acid (EDTA) as masking agents.[30] They observed little or no optical response to other types of ions. Similarly, Li *et al.* used sodium hyaluronate-capped Au NPs for the detection of Cr(III) based on the absorbance ratio of two LSPR peaks at two different wavelengths (A_{650}/A_{525}) obtained after analyte-induced aggregation.[35] Long *et al.* applied colorimetric determination of Cr(III) by synergistic aggregation of Au NPs in the presence of thiourea.[7] Mukherjee and coworkers demonstrated individual and simultaneous detection of Cr(VI) and Cr(III) based on fluorescence quenching of Au NPs caused by aggregation in the presence of Cr(III).[34] Once aggregated, the close proximity of the Au NPs results in a gradual decrease in fluorescence intensity with increasing Cr(III) concentration. It was also observed that common ions, such as Cd^{2+}, Co^{2+}, Cu^{2+}, Fe^{2+}, Pb^{2+}, Hg^{2+}, Mg^{2+}, Al^{3+}, Mn^{2+}, Ni^{2+}, and Zn^{2+} at 1 mM concentration did not result in aggregation of Au NPs while 0.1 μM Cr(III) led to significant aggregation, making the selective detection of Cr(III) possible. The reduction of Cr(VI) to Cr(III) by $NaBH_4$ prior to analysis made it possible to detect both forms of Cr simultaneously. The selective detection of Cr(III) using citrate-coated Au NPs was also achieved in a paper based assay, where citrate-stabilized Au NPs immobilized onto the Whatman filter were allowed to interact with Cr(III) species.[36] Cr(III) selectively caused the aggregation of Au NPs in the presence of other ions, such as Mn^{2+}, Ni^{2+}, Fe^{2+}, Zn^{2+}, Al^{3+}, and Cu^{2+}. A change in color intensity of the Au NPs as a function of analyte concentration allowed the detection of Cr(III) with a detection limit as low as 0.153 μM.

Colorimetric and fluorometric methods of analysis may suffer from matrix interference and they require highly selective complexing agents to cause analyte-induced aggregation of the Au NPs.[37,38] For example, Zhao *et al.* synthesized dithio-carbamate N-benzyl-4-(pyridin-4-ylmethyl)-aniline stabilized Au NPs for colorimetric detection of Cr(III) with a limit of detection of 0.62 μM.[38] Specification of the functionalizing ligand led to remarkable aggregation of Au NPs when exposed to Cr(III), making the detection feasible. Michalski measured trace level concentrations of Cr(III)/Cr(VI) in water samples using an ion exchange chromatography column with UV detection, which adopted strong binding of Cr species.[39]

Both colorimetric and electrochemical methods involve simple instrumentation, high speed, and low cost along with high accuracy in spite of their relatively lower sensitivity.[7,30,40] The detection of Cr and melamine by electrochemical methods are of interest due to

[z]E-mail: f.zamborini@louisville.edu

these potential benefits.[29,40–44] As an example, Korshoj *et al.* fabricated an electrochemical ion sensor based on the electrocatalytic reaction between Cr(VI) and methylene blue (MB).[40] The surface immobilized MB was reduced to leucomethylene blue (LMB) on the electrode surface, whose charge was then monitored by reduction of Cr(VI) to Cr(III) as LMB became oxidized back to MB. Wyantuti *et al.* performed voltammetric detection of Cr(VI) by using a glassy carbon electrode (GCE) modified with Au NPs.[44] Alizadeh *et al.* developed an electrochemical sensing platform using a nano-structured Cr(III) imprinted polymer-modified carbon-composite electrode.[27] They monitored the oxidation of Cr(III) adsorbed into the film by differential pulse voltammetry. Sari *et al.* detected Cr(VI) in river water by cyclic voltammetry (CV) and AC impedance using a graphene/Au NP-modified GCE.[45]

There are several reports of melamine detection by electrochemical methods. Guo *et al.* reported an electrochemical sensor for detection of melamine by forming a copper-melamine complex using an ordered mesoporous carbon-modified GCE with a limit of detection (LOD) down to ~2 nM.[46] Rovina and Siddiquee reported an electrochemical sensor for rapid determination of melamine using ionic liquid/zinc oxide NPs/chitosan/Au electrode with ~0.01 pM LOD.[47] The fabrication and characterization of the sensor was, however, tedious and complicated for routine analysis. Peng *et al.* utilized Au NPs deposited onto a graphene-doped carbon paste electrodes for the selective and sensitive detection of melamine.[48] Strong interactions between Au and melamine led to a decrease in the peak current for the reduction of Au NPs with increasing melamine concentration. The signal was enhanced by differential pulse voltammetry (DPV) with a LOD of ~20 pM. Daizy *et al.* detected melamine at a reduced graphene oxide-copper nanoflowers modified GCE using ascorbic acid (AA) as an active recognition element with a LOD ranging from 10 nM to 90 nM.[42] H-bonding between AA and melamine made it possible to correlate the electrochemical signal from AA to the melamine concentration.

Inspired by previous reports on Au NP aggregation-based colorimetric detection of Cr and melamine and our recent demonstration that the peak potential in the anodic stripping voltammetry (ASV) of citrate-stabilized Au NPs (cit-Au NPs) shifts dramatically positive upon aggregation,[49] we set out to detect Cr^{3+} and melamine by ASV-based detection of analyte-induced Au NP aggregation. Our idea is similar to the recently published work of Zahran and co-workers, who detected 20 ppb atrazine indirectly from the fact that it increased the electrooxidation current of Ag in the ASV by aggregation of cit-Ag NPs.[50] Our method involves selective interactions between Cr^{3+}/melamine and cit-Au NPs followed by fast electrophoretic deposition (EPD) of the Au NPs, and finally ASV to determine the analyte concentration based on the peak current or peak oxidation potential. EPD is a unique aspect of this detection scheme compared to Zahran and co-workers and other previous work. EPD quickly concentrates the Au NPs on the electrode surface, where interactions between the cit-Au NPs and analyte can alter the electrophoretic mobility of the Au NPs. This in turn alters the ASV peak potential and/or peak current. In either detection mode (potential or current), EPD is a critical component that has not been exploited previously.

Experimental

Chemicals and materials.—Sodium borohydride (⩾ 98%), (3-aminopropyl)triethoxysilane (⩾ 98.0%), 2-propanol (ACS reagent), and melamine (99%) were purchased from Sigma Aldrich. $HAuCl_4{\cdot}3H_2O$ was synthesized from metallic Au (99.98%) in our lab. Acetone, methanol, and ethyl alcohol (ACS/USP grade) were purchased from Pharmco-AAPER. Trisodium citrate salt, potassium perchlorate (99.0%–100.5%), and potassium bromide (GR ACS) were purchased from Bio-Rad laboratories, Beantown Chemical, and EMD, respectively. Chromium nitrate was purchased from Fisher Scientific. Hydroquinone (HQ, 99%) was purchased from Alfa Aesar. Indium-tin-oxide (ITO)-coated glass slides (CG-50IN-CUV, R_s = 8–12 Ω) were purchased from Delta Technologies Limited (Loveland, CO).

Synthesis of citrate-coated 4.1 nm and 15.1 nm diameter Au NPs.—We synthesized citrate-coated 4.1 nm average diameter Au NPs (cit-Au NPs) by the method of Murphy and co-workers as described by our group in previous publications.[51–53] We synthesized 15.1 nm cit-Au NPs by the method originally developed by Turkevich as reported in our previous publications.[54–56]

Electrophoretic deposition (EPD) of Au NPs.—50 μL of five different concentrations (0.010, 0.050, 0.10, 0.20, and 0.30 mM) of Cr^{3+} were added to 5 mL of as-synthesized 4.1 and 15.1 nm cit-Au NPs so that the final Cr^{3+} concentrations were 5, 25, 50, 100, and 150 ppb, respectively. After addition of Cr^{3+} solution to the Au NPs, the resulting solution sat for 1 h. A blank sample for both Au NPs was prepared by just adding 50 μL of nanopure water into the 5 mL of as prepared solution of Au NPs. A solution mixture for EPD was then prepared by mixing 2 mL of the Cr^{3+}/Au NP solution, 23 mL of nanopure water, and 5 mL of 0.1 M HQ. Next, EPD was performed for 5 min using a CH Instruments (Austin, TX) model CHI660E electrochemical workstation with a 3-electrode set-up, including the cleaned glass/ITO as the working electrode (dimension = 1.2 cm × 0.7 cm), a Pt wire as the counter electrode, and Ag/AgCl reference electrode. The EPD potential was set at 1.2 V and 1.0 V vs Ag/AgCl (3M KCl) for 15.1 nm and 4.1 nm Au NPs, respectively. The glass/ITO electrode was then removed from the EPD solution, thoroughly rinsed with nanopure water, and finally dried with N_2. For melamine detection, five different aqueous solutions of melamine with concentrations of 0.0080, 0.020, 0.040, 0.080 and 0.12 mM were prepared. Then, 50 μL of each was added to 5 mL of nanopure water to obtain solutions with final concentrations of 10, 25, 50, 100 and 150 ppb, respectively. Melamine binds strongly to cit-Au NPs due to the presence of three NH_2 groups resulting in partial surface charge neutralization and/or aggregation of the Au NPs.[57] Experiments for EPD of Au NPs/melamine were performed under similar conditions as in the case of Au NPs/Cr^{3+}, where the EPD solution consisted of 2 mL of the melamine/Au NPs solution, 23 mL of nanopure water, and 5 mL of 0.1 M HQ. EPD was performed at the same potential and time as for Cr^{3+} detection and the glass/ITO was rinsed and dried in the same way.

ASV characterization.—ASV was performed with a CH Instruments CHI660E electrochemical workstation using glass/ITO/Au NPs (after EPD) as the working electrode, a Pt wire counter electrode, and an Ag/AgCl reference electrode. The peak potential (E_p) and area under the peak (in Coulombs) for Au NP oxidation by Br^- was determined by scanning linearly from 0.0 V to 1.2 V at a scan rate of 0.01 V s^{-1} in 0.01 M KBr plus 0.1 M $KClO_4$ electrolyte solution.

UV–vis characterization.—Ultraviolet–visible spectrometry (UV–vis) was performed using a Varian Instruments Cary 50 Bio-spectrophotometer. UV–vis spectra were obtained from 350 – 900 nm in aqueous solutions of different-sized Au NPs using water as the blank.

Results and Discussion

Detection strategy.—The main goal of this work was to develop a simple, cheap, and sensitive electrochemical method that combines selective interactions between analyte and ligand-stabilized metal NPs with electrophoretic deposition (EPD) and anodic stripping voltammetry (ASV) analysis. Scheme 1 shows the general analysis strategy. Step 1 involves the synthesis of ligand-stabilized Au nanoparticles (NPs) and step 2 requires mixing of the Au NPs with the analyte of interest, where there is some selective affinity between the analyte and ligand stabilizer. In this work, citrate-stabilized Au NPs (cit-Au NPs) selectively bind to Cr^{3+} ions or

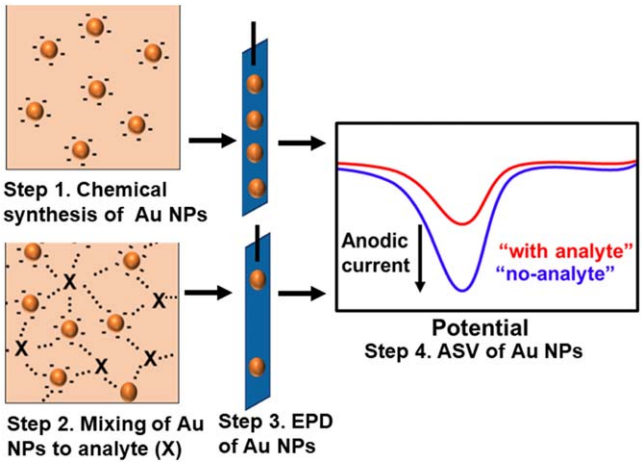

Scheme 1. General experimental work-flow in this project.

melamine as the analyte.[35,42] In step 3, we perform EPD of the cit-Au NPs in the absence and presence of various analyte concentrations under defined EPD conditions (constant potential and time) using the method of Allen *et al.*, who recently described the EPD of cit-Au NPs in the presence of hydroquinone (HQ).[49] The number of cit-Au NPs deposited depends on the electrophoretic mobility, which depends on the charge/size ratio of the cit-Au NPs. The negative charge can be decreased by neutralizing the carboxylate groups of citrate with Cr^{3+} and melamine (NH_3^+ groups) and the size can potentially be increased by Cr^{3+}- or melamine-induced aggregation of the Au NPs.[34,42] Both processes would lead to reduced electrophoretic mobility, leading to a lower amount of deposited cit-Au NPs onto the glass/ITO electrode surface as shown in the step 3 illustration. Finally, in step 4 we use ASV to determine the amount of cit-Au NPs deposited by EPD by integrating the charge under the peak corresponding to Au oxidation by Br^- according to reactions 1 and 2 (primarily reaction 1).[56]

$$Au^0 + 4Br^- \rightarrow AuBr_4^- + 3e^- (E^0 = 0.85 \text{ Vvs NHE}) \quad [1]$$

$$Au^0 + 2Br^- \rightarrow AuBr_2^- + e^- (E^0 = 0.96 \text{ V vs NHE}) \quad [2]$$

Based on the proposed mechanism, the integrated charge of the Au oxidation peak in ASV should decrease as the analyte concentration increases as shown in the illustration in step 4. The analytical signal, which is the change in peak charge ($\Delta Q_{peak} = Q_{blank} - Q_{analyte}$), is plotted versus the analyte concentration. The peak oxidation potential (E_p) could also shift to higher potentials if the analyte induces significant aggregation of Au NPs, according to our previous work[49] and recent report by Zahran *et al.*[50]

Cr^{3+} Detection.—Figure 1A shows ASVs of 15.1 nm cit-Au NPs obtained after exposure to different concentrations of Cr^{3+} for 1 h followed by EPD at 1.2 V (vs Ag/AgCl) for 5 min as described in the experimental section. The peak oxidation potential (E_p) at 0.78 V is due to Au oxidative dissolution by Br^-. The peak current and integrated charge under the peak clearly decrease as the concentration of Cr^{3+} increases as expected based on the potential mechanisms already described. The average charge under the peak for 0 ppb Cr^{3+} was 47.8 ± 1.4 μC while that with 5, 25, 50, 100 and 150 ppb Cr^{3+} was 43.1 ± 3.2, 36.5 ± 1.8, 32.4 ± 2.6, 25.9 ± 2.2, and 17.9 ± 2.0 μC, respectively. We believe the signal is dominated by Cr^{3+} neutralization of citrate as opposed to Cr^{3+}-induced aggregation, since the E_p does not change dramatically. Alternatively, the cit-Au NPs may aggregate with spacing between the Au NPs, where the surface area-to-volume ratio (SA/V) of the Au NPs does not change significantly.[58] A third possibility is that aggregation occurs in solution, but the aggregated Au NPs do not deposit onto the

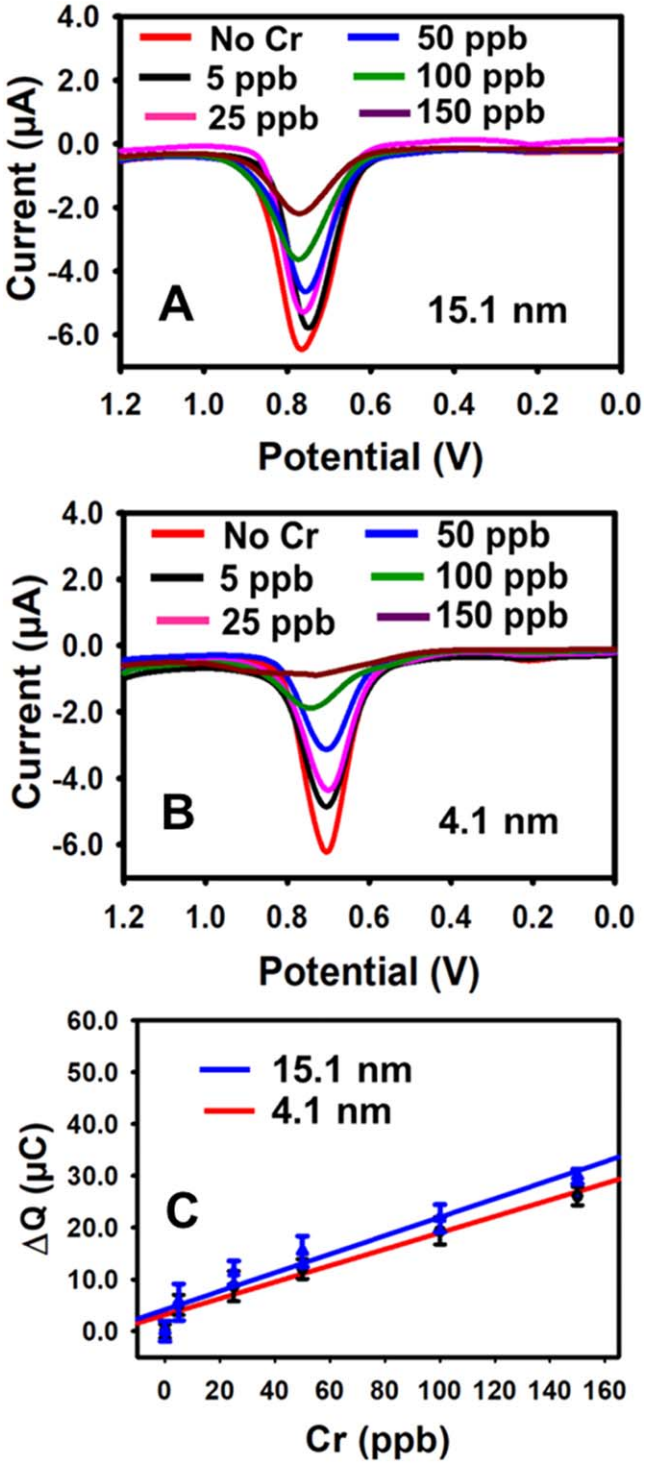

Figure 1. ASV signature of 15.1 nm (A) and 4.1 nm (B) Au NPs treated with different Cr^{3+} concentrations followed by EPD. Calibration curve plotting the difference in Au stripping charge of Au NPs with and without Cr^{3+} (ΔQ) versus Cr^{3+} concentration for 15.1 nm (blue) and 4.1 nm (red) cit-Au NPs (C).

electrode during EPD, causing a lowering of the Au stripping signal. The binding event occurs due to the chelating nature of Cr^{3+}, where a pair of Au NPs can be cross linked by a single Cr^{3+} ion via the negatively-charged carboxylate and hydroxyl group.[59] The chelating behavior of Cr^{3+} is highly specific over other positively-charged ions, such as Cu^{2+}, Pb^{2+}, Fe^{3+} , and Al^{3+}.[34]

Under identical conditions, we used 4.1 nm cit-Au NPs for the detection of $Cr.^{3+}$ We also found a decrease in peak current and Au oxidative charge with increasing Cr^{3+} concentration (Fig. 1B). The oxidative charge was 33.1 ± 1.0, 28.0 ± 1.7, 24.4 ± 2.8, 21.1 ± 1.6, 13.7 ± 2.5 and 7.0 ± 1.5 μC, for 0, 5, 25, 50, and 150 ppb Cr^{3+}, respectively. The response is due to the same mechanism described for 15.1 nm cit-Au NPs.

Table I displays the average Au electrooxidation charges obtained from ASV peak integration for 15.1 nm and 4.1 nm diameter cit-Au NPs after EPD in the presence of different concentrations of Cr^{3+} (The charges for individual samples are provided in Table SI (available online at stacks.iop.org/JES/169/016504/mmedia)). Figure 1C shows the calibration curves plotting the average ΔQ_{peak} as a function of Cr^{3+} concentration using both Au NP sizes. We found a linear dependence with a positive slope, where the ΔQ_{peak} increases with increasing Cr^{3+} concentration with an R^2 value of 0.947 and 0.966 for 15.1 and 4.1 nm cit-Au NPs, respectively. The sensitivity, as determined by the slope of the calibration curve, is 0.19 μC/ppb and 0.17 μC/ppb for 15.1 and 4.1 nm Au NPs, respectively, which are not significantly different. The LOD was estimated by 3 s m^{-1}, where s is the standard deviation of the blank sample and m is the slope of the line of best fit. The limit of detection (LOD) was found to be 21.1 ppb for 15.1 nm Au NPs and 16.0 ppb for 4.1 nm Au NPs, which are also very similar. The EPA recommended level of total Cr in drinking water must be below 100 ppb in order to be safe, showing that this method is capable of detection well below that limit.[60]

We compared the EPD-ASV method to UV–vis spectroscopy for Cr^{3+} detection by monitoring the change in the wavelength of maximum absorbance of the LSPR peak of the Au NPs in the presence of different concentrations of Cr^{3+}. For 15.1 nm Au NPs (Fig. 2A), we observed a variation in peak absorbance at ~518 nm for different Cr^{3+} concentration (details in Table SII). The absorbance was 0.499 ± 0.016, 0.482 ± 0.053, and 0.493 ± 0.023 for 0, 100, and 150 ppb of Cr^{3+}, respectively. This very small change in absorbance was not statistically significant for analysis considering the variability and lack of a trend. However, a small shoulder peak on the UV–vis spectra was observed with an increase in Cr^{3+} concentration in the wavelength range from 550 nm to 900 nm. We therefore constructed a calibration curve of absorbance at 650 nm versus Cr^{3+} concentrations (Fig. 2D, blue plot), which gave a sensitivity of 0.00069 a.u./ppb and LOD of 22.2 ppb for the 15.1 nm Au NPs. We also monitored the UV–vis spectra of 4.1 nm Au NPs with varying Cr^{3+} concentration (Fig. 2B). A decrease in peak absorbance occurred at 505 nm with increasing Cr^{3+} concentration, which was not insignificant as it was in the case of 15.1 nm Au NPs. Figure 2C shows a calibration curve of ΔA_{505} as a function of Cr^{3+} concentration, which had a sensitivity of ~0.00058 a.u./ppb and calculated LOD of 39.3 ppb. Similarly, we plotted the peak absorbance at 650 nm for 4.1 nm Au NPs as a function of Cr^{3+} concentration (Fig. 2D, red plot), which showed a sensitivity of 0.00048 a.u./ppb and LOD of 29.4 ppb. The sensitivity and LOD for the EPD-ASV measurement was slightly better, but comparable with the UV–vis methods.[37,60]

Melamine detection.—We next applied the EPD-ASV method to the detection of melamine, a biologically-relevant molecule, using 4.1 nm diameter cit-Au NPs. Melamine binds strongly to cit-Au NPs due to the presence of three -NH_2 groups resulting in partial surface charge neutralization and/or aggregation of the Au NPs.[57] We observed that the area under the ASV peak decreased with increasing melamine concentration (Fig. 3A) as it did with Cr^{3+}. Interestingly, the peak oxidation potential also increased to some extent with increasing melamine concentration beyond 50 ppb (Fig. 3A), suggesting that there was small aggregation of the cit-Au NPs in the presence of melamine. This leads to a positive shift in the oxidation potential due to a reduced surface area-to-volume ratio (SA/V) of the cit-Au NPs after aggregation.[49,56] Binding with Cr^{3+}, on the other hand, does not seem to alter the SA/V of the Au NPs since the peak potential did not change significantly. The three -NH_2 groups in melamine interact with the cit-Au NPs, causing the dissociation of citrate ions from the surface of Au NPs, leading to aggregation with close Au-Au NP contacts.[61] The extent of aggregation and citrate charge neutralization depends on the concentration of melamine, leading to a decrease in the amount of Au NPs deposited by EPD with increasing analyte concentration as determined by ASV. Figure 3B shows a calibration curve of ΔQ_{peak} as a function of melamine concentration, which has a R^2 value of 0.976 and LOD of 45.7 ppb melamine. This is significantly lower than the EPA recommended lower limit of melamine (2.5 ppm) required for safe food and water.[17]

We next monitored the variation in UV–vis absorbance of 4.1 nm Au NPs with varying melamine concentration (Fig. 3C). We observed a peak absorbance decrease at 505 nm and absorbance increase at 650 nm (details of the absorbance values in Table SII). A plot of ΔA_{650} of 4.1 nm Au NPs against melamine concentration is shown in Fig. 3D. Based on the curve, we calculated a sensitivity of 0.00096 a.u./ppb and LOD of 40.06 ppb. The LOD of melamine is comparable with both the EPD-ASV and UV–vis methods.

Decreasing limit of detection (LOD) of the method.—Finally, we further decreased the limit of detection of Cr^{3+} by diluting the as-prepared 4.1 nm Au NPs by a factor of 10 followed by addition of 50 μL of 0.002 mM Cr^{3+} (1 ppb Cr^{3+} concentration) and subsequent EPD and ASV at the same potential for the same time. This variation increased the Cr^{3+}/Au ratio in the solution by a factor of 10 with 1 ppb of Cr^{3+}. Under identical conditions, the charges of Au obtained from ASV in presence of 1 ppb of Cr^{3+} was found to be 25.4 ± 1.4 μC while that without Cr^{3+} was 31.1 ± 1.3 μC, which are statistically different at 95% confidence using a t-test. Our result shows that detection of Cr^{3+} even down to the 1 ppb level is possible by this approach which is nearly 10-fold less than the LOD obtained under our initial conditions. This demonstrates the success of improvement in the LOD with our method by simply increasing the Cr^{3+}/Au NP ratio. The LOD could be decreased further by optimization of the Cr^{3+}/Au ratio, Au NP-analyte binding time, and EPD potential and time.

Table I. Integrated charges obtained by electrooxidation of 15.1 and 4.1 nm Au after EPD for different concentration of Cr^{3+}.

Cr^{3+} concentration (ppb)	15.1 nm Au stripping charges ± S.D. (μC)	4.1 nm Au stripping charges ± S.D. (μC)
0	47.8 ± 1.4	33.1 ± 1.0
5	43.1 ± 3.2	28.0 ± 1.7
25	36.5 ± 1.8	24.4 ± 2.8
50	32.4 ± 2.6	21.1 ± 1.6
100	25.9 ± 2.2	13.6 ± 2.5
150	17.9 ± 2.0	7.0 ± 1.5

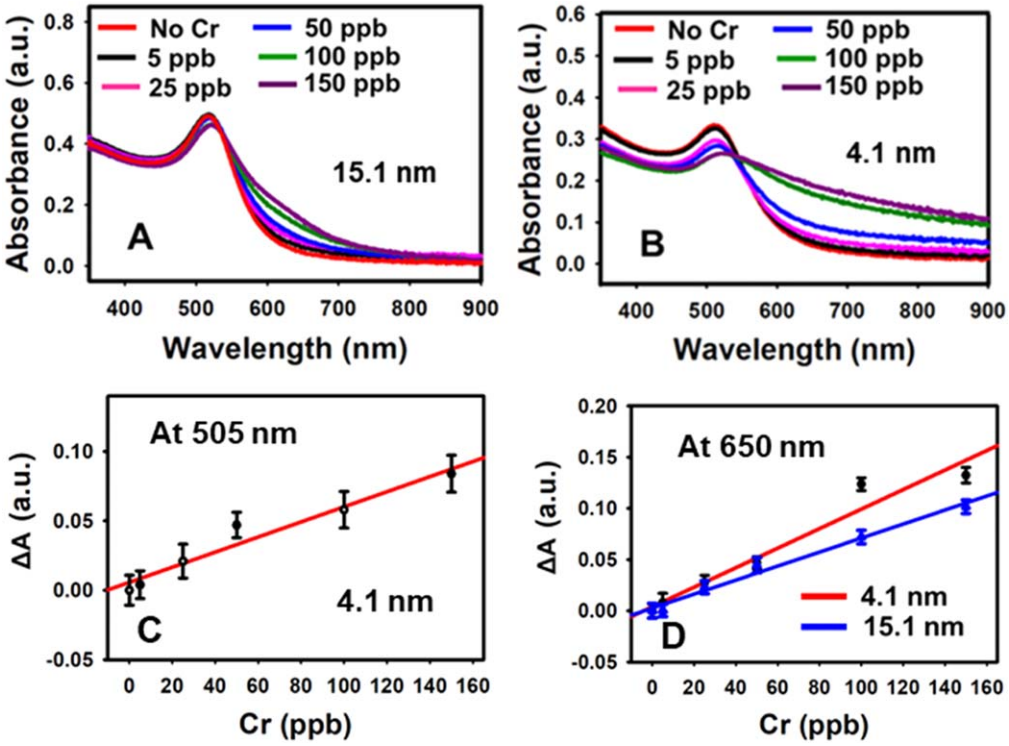

Figure 2. UV–Vis of 15.1 nm (A) and 4.1 nm (B) of Au NPs treated with different Cr^{3+} concentration. Calibration curve of deviation in UV–Vis absorbance at 505 nm of 4.1 nm Au NPs with different Cr^{3+} concentration from sample with no Cr^{3+} (ΔA) versus Cr^{3+} concentration (C) and calibration curve of deviation in UV–Vis absorbance at 650 nm of 15.1 nm (blue) and 4.1 nm (red) Au NPs at different Cr^{3+} concentration from sample with no Cr^{3+} versus Cr^{3+} concentration (D).

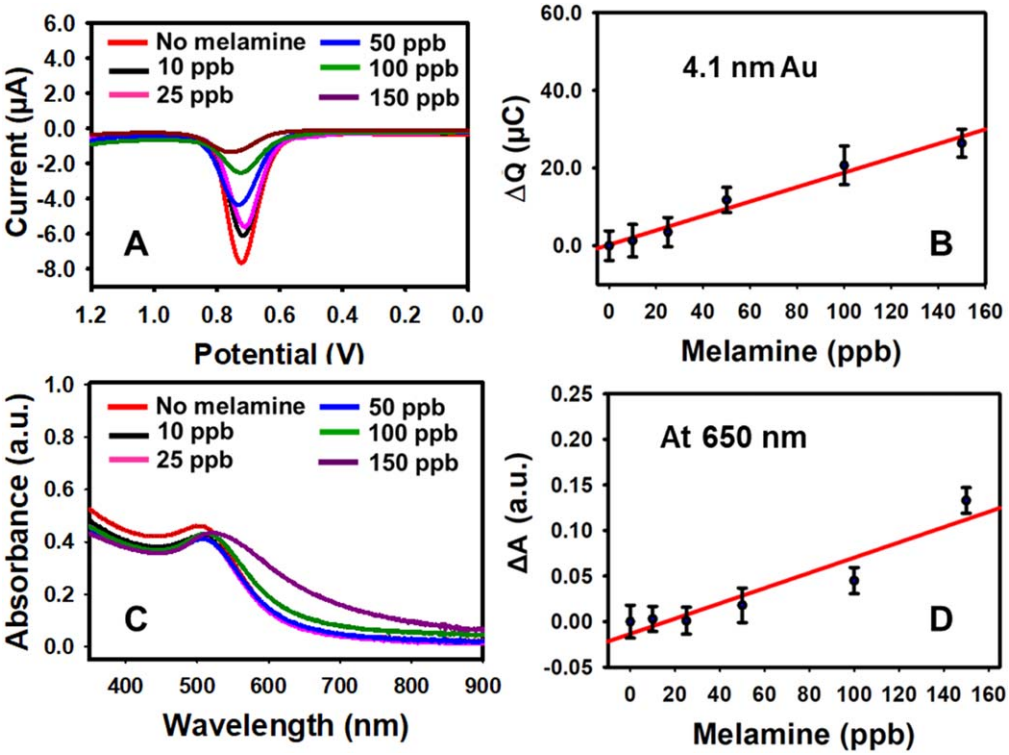

Figure 3. ASV signature of 4.1 nm Au NPs treated with different melamine concentration followed by EPD (A) and calibration curve of deviation in Au stripping charges from sample with no melamine using ASV of 4.1 nm Au NPs (ΔQ) versus melamine concentration (B). UV–Vis of 4.1 nm Au NPs treated with different melamine concentration (C) and calibration curve of deviation in UV–Vis absorbance of 4.1 nm Au NPs at 650 nm from sample with no melamine (ΔA) versus melamine concentration (D).

Conclusions

We described a unique electrochemical method for the detection of Cr^{3+} and melamine by selective binding of analyte to cit-Au NPs followed by EPD of the cit-Au NPs and stripping of the Au by ASV. The ASV peak charge decreases linearly with increasing concentration based on reduced cit-Au NP electrophoretic mobility upon analyte binding due to reduced charge of the NPs or increased size caused by analyte-induced aggregation. Another possible mechanism is that analyte binding lowers the catalytic activity of the Au NPs towards oxidation of HQ which in turn decreases the extent of Au deposited on the electrode during EPD or that analyte-induced aggregation simply lowers the concentration of free Au NPs in solution for EPD. The ASV peak potential may also increase upon analyte-induced binding and aggregation, as observed slightly for melamine, but this is not extensive enough to be used as the analytical signal. Importantly, the citrate ligands show high selectivity for Cr^{3+} ions, the EPD is reproducible, and the change in peak charge with concentration is highly sensitive. The limit of detection is in the 10–50 ppb range for both Cr^{3+} and melamine, which is sufficient for environmental applications. The analysis takes about 1 h to complete with similar analytical merits as UV–vis or fluorescence-based detection utilizing Au and Ag NPs. Our method has the potential advantage of being useful for non-plasmonic metal NPs and metal NPs of 2 nm and below, which do not exhibit a LSPR band. Further optimization is also possible to improve the LOD to 1 ppb and possibly below that in the future.

Acknowledgments

We gratefully acknowledge the National Science Foundation (NSF) for financial support of this research through Grant CHE-1611170 and CHE-2004169.

ORCID

Francis P Zamborini https://orcid.org/0000-0003-0685-0180

References

1. M. B. Arain;, I. Ali;, E. Yilmaz;, and M. Soylak, *Trends Anal. Chem.*, **103**, 44 (2018).
2. W. Jin and K. Yan, *RSC Adv.*, **5**, 37440 (2015).
3. A. Zhitkovich, *Chem. Res. in Toxicol.*, **24**, 1617 (2011).
4. M. Zhan, H. Yu, L. Li, D. T. Nguyen, and W. Chen, *Anal. Chem.*, **91**, 2058 (2019).
5. D. Rai, B. M. Sass, and D. A. Moore, *Inorg. Chem.*, **26**, 345 (1987).
6. A. D. Dayan and A. J. Paine, *Hum. Exp. Toxicol.*, **20**, 439 (2001).
7. D. Long and H. Yu, *Anal. Bioanal. Chem.*, **408**, 8551 (2016).
8. W. Zhou, T. Yu, M. Vazin, J. Ding, and J. Liu, *Inorg. Chem.*, **55**, 8193 (2016).
9. O. Y. Vasylkiv, O. I. Kubrak, K. B. Storey, and V. I. Lushchak, *Chemosphere*, **80**, 1044 (2010).
10. E. Rifkin, P. Gwinn, and E. Bouwer, *Environ. Sci. Technol.*, **38**, 267 (2004).
11. D. M. Hausladen and S. Fendorf, *Environ. Sci. Technol.*, **51**, 2058 (2017).
12. T.-H. Tsai, S. Thiagarajan, and S.-M. Chen, *J. Agric. Food Chem.*, **58**, 4537 (2010).
13. Y. Liu, E. E. D. Todd, Q. Zhang, J.-R. Shi, and X.-J. Liu, *J. Zhejiang Univ. Sci. B*, **13**, 525 (2012).
14. A. K.-C. Hau, T. H. Kwan, and P. K.-T. Li, *J. Am. Soc. Nephrol.*, **20**, 245 (2009).
15. Y. Lu, Y. Xia, G. Liu, M. Pan, M. Li, N. A. Lee, and S. Wang, *Critical Rev. Anal. Chem.*, **47**, 51 (2017).
16. C. M.-E. Gossner, J. Schlundt, P. B. Embarek, S. Hird, D. Lo-Fo-Wong, J. J. O. Beltran, K. N. Teoh, and A. Tritscher, *Env. Health Persp.*, **117**, 1803 (2009).
17. European Food Safety Authority, "Scientific Opinion on Melamine in Food and Feed." *EFSA J.*, **8**, 1573 (2010).
18. R. M. Cespón-Romero, M. C. Yebra-Biurrun, and M. P. Bermejo-Barrera, *Anal. Chim. Acta*, **327**, 37 (1996).
19. Z. Sun and P. Liang, *Microchim. Acta*, **162**, 121 (2008).
20. J. Peng, Y. He, L. Ye, T. Shen, F. Liu, W. Kong, X. Liu, and Y. Zhao, *Anal. Chem.*, **89**, 7593 (2017).
21. T. Zhang, S. Zhang, J. Liu, J. Li, and X. Lu, *Anal. Chem.*, **92**, 3426 (2020).
22. N. Martone, G. M. M. Rahman, M. Pamuku, and H. M. S. Kingston, *J. Agric. Food Chem.*, **61**, 9966 (2013).
23. F. Séby, S. Charles, M. Gagean, H. Garraud, and O. F. X. Donard, *J. Anal. Atom. Spec.*, **18**, 1386 (2003).
24. Y. B. Yin, C. L. Coonrod, K. N. Heck, F. Lejarza, and M. S. Wong, *ACS Appl. Mater. Interfaces*, **11**, 17491 (2019).
25. X. Li, S. Zhang, Y. Dang, Z. Liu, Z. Zhang, D. Shan, X. Zhang, T. Wang, and X. Lu, *Anal. Chem.*, **91**, 4031 (2019).
26. M. Farrokhnia, S. Karimi, and S. Askarian, *ACS Sustain. Chem. Eng.*, **7**, 6672 (2019).
27. T. Alizadeh, F. Rafiei, N. Hamidi, and M. R. Ganjali, *Electrochim. Acta*, **247**, 812 (2017).
28. A. Prakash, S. Chandra, and D. Bahadur, *Carbon*, **50**, 4209 (2012).
29. L. Zhu, M. Miao, X. Shao, Z. Du, K. Huang, Y. Luo, and W. Xu, *Anal. Chem.*, **91**, 14992 (2019).
30. C. Dong, G. Wu, Z. Wang, W. Ren, Y. Zhang, Z. Shen, T. Li, and A. Wu, *Dalton Trans.*, **45**, 8347 (2016).
31. K. Ai, Y. Liu, and L. Lu, *J. Am. Chem. Soc.*, **131**, 9496 (2009).
32. X. Zhang, W. Liu, X. Li, Z. Zhang, D. Shan, H. Xia, S. Zhang, and X. Lu, *Anal. Chem.*, **90**, 14309 (2018).
33. Y.-T. Zhuang, S. Chen, R. Jiang, Y.-L. Yu, and J.-H. Wang, *Anal. Chem.*, **91**, 5346 (2019).
34. E. Mathivanan, S. A. Alex, N. Chandrasekaran, and A. Mukherjee, *Anal. Methods*, **6**, 9554 (2014).
35. S. Li, T. Wei, G. Ren, F. Chai, H. Wu, and F. Qu, *Colloids Surf. A*, **535**, 215 (2017).
36. E. Mathivanan, R. A.;. N. Chandrasekaran, and A. Mukherjee, *Anal. Methods*, **5**, 6211 (2013).
37. G. Liu, M. Lu, X. Huang, T. Li, and D. Xu, *Sensors*, **18**, 4166 (2018).
38. L. Zhao, Y. Jin, Z. Yan, Y. Liu, and H. Zhu, *Anal. Chim. Acta*, **731**, 75 (2012).
39. R. Michalski, *J. Liq. Chromatogr. Relat.*, **28**, 2849 (2005).
40. L. E. Korshoj, A. J. Zaitouna, and R. Y. Lai, *Anal. Chem.*, **87**, 2560 (2015).
41. S. Wyantuti, Y. W. Hartati, C. Panatarani, and R. Tjokronegoro, *Procedia Chem.*, **17**, 170 (2015).
42. M. Daizy, C. Tarafder, M. R. Al-Mamun, X. Liu, M. Aly Saad Aly, and M. Z. H. Khan, *ACS Omega*, **4**, 20324 (2019).
43. D. K. Pattadar, J. N. Sharma, B. P. Mainali, and F. P. Zamborini, *Curr. Opin. Electrochem.*, **13**, 147 (2019).
44. S. Wyantuti, S. Ishmayana, and Y. W. Hartati, *Procedia Chem.*, **16**, 15 (2015).
45. T. K. Sari, F. Takahashi, J. Jin, R. Zein, and E. Munaf, *Anal. Sci.*, **34**, 155 (2018).
46. Z. Guo, Y.-T. Zhao, Y.-H. Li, T. Bao, T.-S. Sun, D.-D. Li, X.-K. Luo, and H.-T. Fan, *Food Anal. Methods*, **11**, 546 (2018).
47. K. Rovina and S. Siddiquee, *Food Control*, **59**, 801 (2016).
48. J. Peng, Y. Feng, X.-X. Han, and Z.-N. Gao, *Anal. Methods*, **8**, 2526 (2016).
49. S. L. Allen, J. N. Sharma, and F. P. Zamborini, *J. Am. Chem. Soc.*, **139**, 12895 (2017).
50. M. Zahran, Z. Khalifa, M. A. H. Zahran, and M. Abdel Azzem, *ACS Appl. Nano Mater.*, **3**, 3868 (2020).
51. N. R. Jana, L. Gearheart, and C. J. Murphy, *J. Phy. Chem. B*, **105**, 4065 (2001).
52. B. P. Mainali, D. K. Pattadar, and F. P. Zamborini, *J. Phys. Chem. C*, **125**, 2719 (2021).
53. B. P. Mainali, D. K. Pattadar, and F. P. Zamborini, *J. Electrochem. Soc.*, **167**, 146503 (2020).
54. J. Turkevich, P. C. Stevenson, and J. Hillier, *Discuss. Faraday Soc.*, **11**, 55 (1951).
55. D. K. Pattadar, J. N. Sharma, B. P. Mainali, and F. P. Zamborini, *J. Phys. Chem. C*, **123**, 24304 (2019).
56. J. N. Sharma, D. K. Pattadar, B. P. Mainali, and F. P. Zamborini, *Anal. Chem.*, **90**, 9308 (2018).
57. F. Wei, R. Lam, S. Cheng, S. Lu, D. Ho, and N. Li, *Appl. Phys. Lett.*, **96**, 133702 (2010).
58. D. K. Pattadar, H. N. Nambiar, S. L. Allen, J. B. Jasinski, and F. P. Zamborini, *Langmuir*, **37**, 7320 (2021).
59. Y. Ye, H. Liu, L. Yang, and J. Liu, *Nanoscale*, **4**, 6442 (2012).
60. S. Shahim, R. Sukesan, I. Sarangadharan, and Y.-L. Wang, *Sensors*, **19**, 1969 (2019).
61. K. Chang, S. Wang, H. Zhang, Q. Guo, X. Hu, Z. Lin, H. Sun, M. Jiang, and J. Hu, *PLoS One*, **12**, 177131 (2017).